# Ideal-System Morphology and Reflectivity Measurements for Radiative-Transfer Model Development and Validation

T.J.Kulp*[,a], R.L. Sommers[a], K.L. Krafcik[a], B.E. Mills[a], T.A. Reichardt[a],
J.K. Dorrance[a], C.F. LaCasse IV[b], K.H. Fuerschbach[b], and J. Craven[b]
Sandia National Laboratories; [a]7011 East Ave. Livermore CA, 94551,
and [b]1515 Eubank SE, Albuquerque, NM 87123
*tjkulp@sandia.gov; phone 925-294-3676

## ABSTRACT

This paper describes measurements being made on a series of material systems for the purpose of developing a radiative-transfer model that describes the reflectance of light by granular solids. It is well recognized that the reflectance spectra of granular materials depend on their intrinsic (n(λ) and k(λ)) and extrinsic (morphological) properties. There is, however, a lack of robust and proven models to relate spectra to these parameters. The described work is being conducted in parallel with a modeling effort[1] to address this need. Each follows a common developmental spiral in which material properties are varied and the ability of the model to calculate the effects of the changes are tested. The parameters being varied include particle size/shape, packing density, material birefringence, optical thickness, and spectral contribution of a substrate. It is expected that the outcome of this work will be useful in interpreting reflectance data for hyperspectral imaging (HSI), and for a variety of other areas that rely on it.

**Keywords:** Times Roman, image area, acronyms, references

## 1. INTRODUCTION

The remote detection of solid materials (Fig. 1) using hyperspectral imaging (HSI) is an active area of research for defense and industrial monitoring applications[1]. The measurement of condensed-phase materials is a natural outgrowth of earlier activities focusing on gas detection. It is accompanied, however, by the need to employ material library spectra that exhibit far more variability than those of gases. The interaction of a molecular gas with light is defined by a single absorbance spectrum (k(λ)) that determines its volumetric absorbance and emittance. In contrast, solids are typically multiphase aggregates that interact with light through a complex radiative-transfer (RT) process (Fig. 2) whose outcome is described by the overall reflectance (and emittance) spectrum of the assembly. It is well recognized[2-8] that the spectrum of a particular solid species is determined by extrinsic material properties (particle size and shape, packing density, optical thickness), as well as intrinsic (n(λ) and k(λ)) ones. Thus, a comprehensive spectral library entry for a given solid material must consist of many reflectance spectra, each representing a particular extrinsic state of the material.

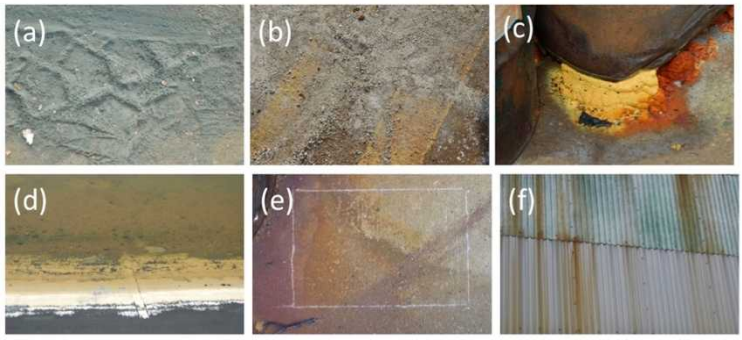


Figure 1 – Typical solid material types for HSI detection, consisting of (a) optically thick powders, (b) optically thin powders, densely packed wet (c) and dry (d) solids, and thin layers on concrete (e) and steel (f) substrates.

The work described here is being conducted in tandem with a theoretical/computational effort whose objective is to create a predictive RT model of solid reflectance spectra. The RT process can be compared to light interactions with

less-dense solids, such as isolated aerosols, or aerosol clouds. The amplitude and scattering pattern (phase) of individual aerosols is determined by single-scatter solutions such as Mie theory (for spheres) which are based on the assumption of a specific particle shape, and which require input of the particle size and its refractive index spectra (n(λ) and k(λ). Solutions for relatively dense clouds of particles must consider the possibility that multiple scattering occurs among many aerosols. Those for a granular solid must consider the effects of close particle-particle proximity on the scattering and attenuation properties of the medium. The latter solutions can be obtained by exact solutions of Maxwell's equations (for small systems) and by "patched" solutions of the RT equation. The latter approach is being pursued by this project, as described in Reference 9.

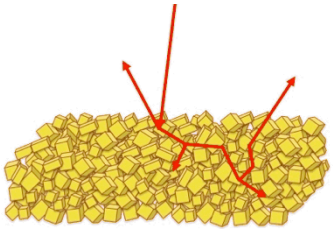

Figure 2 – Diagram depicting the RT process defining the reflectance of light by a granular solid. Some incident radiation is reflected at the surface of the packed medium, while a portion of the rest is diffusely reflected from its interior.

The fabrication and measurement of "ideal" material systems is useful for the development and evaluation of RT models. The control of material attributes afforded by them allows the effect of specific material parameters on RT and reflectance to be quantified and compared to predictions made by a model. This project is adopting a developmental spiral in which the model development and the lab measurements are investigating materials of increasing complexity, which replicate aspects of the "real" materials shown in Fig. 1. As illustrated in Fig. 3, the spiral follows a trajectory in which material systems exhibiting variations of particle size and shape, packing density, surface roughness, optical thickness, birefringence, and spectral contribution from a substrate are constructed and characterized. Accurate modeling of all these dependencies is critical to the modeling of reflectance of the material types of Fig. 1.

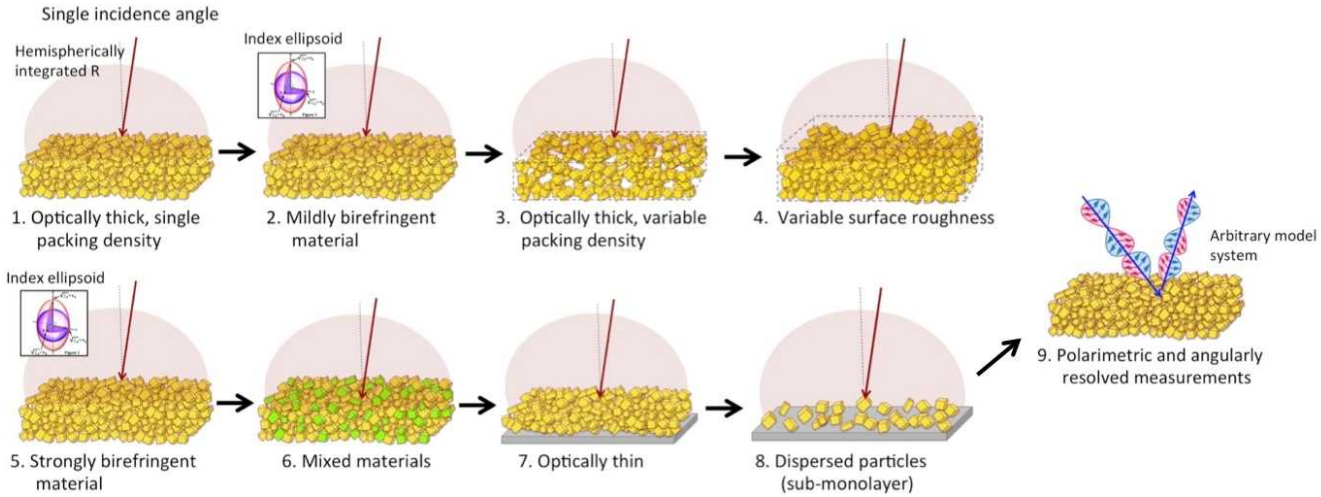


Figure 3 – Diagram of the developmental modeling/measurement spiral being pursued in this project. Each is labeled according to the morphological condition being tested. Systems 1-8 are characterized using directional-hemispherical reflectance measurements; System 9 will be characterized using polarized directional reflectance measurements.

## 2. CHARACTERIZATION METHODS

### 2.1 Morphological characterization

The morphology of a granular solid can be described by the size and shape distributions of the particles that it is composed of, and by the arrangement of the particles as they are packed into an aggregate bed. Sophisticated tools are available to characterize size distributions using optical scattering and automated optical microscopy. Shape

distributions are also obtained using the latter. Emerging tools are extremely useful for full characterization of the morphology of packed solids.

In this project, we employ both an optical scattering instrument (Micromeritics Saturn Digisizer II, Micromeritics Instruments, Norcross GA) and an automated optical microscope (Malvern Morphologi G3, Malvern Instruments, Malvern UK). Each conducts measurements that are averaged over large ensembles ($10^3$ – $10^4$) of particles. The scattering instrument obtains a size distribution by fitting the angular scattering pattern that is observed when a single-wavelength laser beam probes a volume in a fluid containing suspended particles. It is, therefore, limited by assumptions associated with the Mie-scattering model (spherical particles, best available n, k data). Measurements are possible between particle diameters of 0.04 and 2500 μm. The microscopy system scans for, and images, many individual particles that have been deposited on a glass surface. It is limited by diffraction to measurement of particle sizes above 0.5 μm (up to 5000 μm). It is not constrained by assumptions associated with a model (as in the Mie fitting); however, it requires care in setting contrast thresholds that determine particle edges, and can be biased by the requirement that particles lay flat on a surface. Particle dimensions are determined by applying shape models to the thresholded particle images. These models can also quantify the distribution of various morphological parameters (e.g. circularity, ellipticity, etc.) that describe particle shape.

The arrangement of the characterized particle populations within the packed solid is relevant to RT models based on "patched" solutions of the RT equation[9], and to those based on direct solutions of Maxwell's equations[10]. The former typically use particle pair-distribution functions (pdf's) to describe mass distribution within the solid. The pdf (Fig. 4) indicates the probability of finding another particle as a function of radial distance from a given particle in the packed solid. The patched RT model assumes a particular particle shape in conjunction with an analytical form of the pdf appropriate to that shape. For example, the Percus-Yevick[11] pdf is used for spherical particles. RT models based on Maxwell's solution equations can use arbitrary digitized distributions of mass.

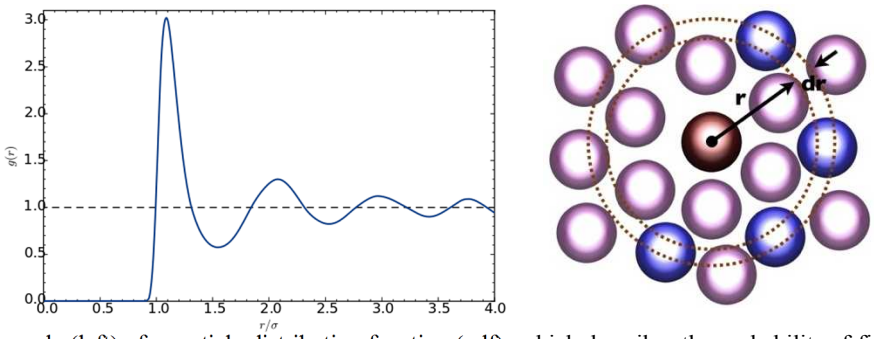


Figure 4 – Example (left) of a particle distribution function (pdf), which describes the probability of finding a particle at some radial distance (units of particle diameter) from a reference particle. (Images from Ref. 12)

Alternate methods of depicting mass distributions might employ either (1) computed distributions calculated using measured particle shape "libraries", or (2) direct measurements of the distribution in a real sample. A path toward the former would be to generate the library by extrapolating microscopically measured particle shapes from two to three dimensions, and then by applying object-packing software (e.g. Rocpack, www.illinoisrocstar.com) to create a digitally depicted packed bed. An example of the latter, which is being pursued in this project, is the measurement of the internal structure of the packed bed using x-ray tomography (XRT). The XRT instrument directly measures the three-dimensional internal structure of exemplary packed samples (e.g., of volumes corresponding to one-to-few mm diameter) with accurate shape determination of particles having diameters as small as a few μm.

### 2.2 Optical characterization

The reflectance of the ideal systems has been characterized using directional-hemispherical reflectance measurements. This is accomplished using an FTIR spectrometer (Digilab FTS 7000) that is coupled to a modified roughened-gold, downlooking integrating sphere (Pike Mid-IR IntegratIR). The measurements are calibrated using reference to an internal reflection in the sphere. Measurements are made in both diffuse reflectance mode (specular component released from the sphere) and total reflectance mode (specular component retained and measured). The quality of the measurement is assessed by measuring samples provided by NIST[13], and comparing them to NIST-generated data.

As indicated in Fig. 3, directional-hemispherical measurements are planned for spiral steps 1-8. Step 9 will implement polarized directional-directional measurements. This will be accomplished using an FTIR (Bruker Vertex 70) that is coupled to a home-built optical assembly that will direct the incident and reflected beams.

## 3. OPTICALLY THICK AND MILDLY BIREFRINGENT IDEAL SYSTEMS

Two steps on the measurement portion of the spiral of Fig. 3 have been accomplished – the optically thick (isotropic) system of Step 1 and the "mildly birefringent" system of Step 2. The results are described below. The following section presents a comparison of the measurement and modeling results for Step 1.

### 3.1 Step 1 – Optically thick, isotropic system

Fused silica was selected as an isotropic (non-birefringent) material for this step of the spiral. The refractive indices of this material have been characterized by a number of researchers and an aggregate comparison of their results is shown in Fig. 5. Size-segregated samples of pure fused silica were obtained from two manufacturers – Pemco (Niagara Falls, NY) and Washington Mills (WM) (Niagara Falls, NY). In each case, five size cuts were obtained, specified according to the sieve mesh used to select them. They are: 50/100, 100/200, 120/F, 200/F, 325/F, where the mesh sizes correlate to the screen pores as follows – 50 = 297 μm; 100 = 149 μm; 120 = 125 μm; 200 = 74 μm; and 325 = 44 μm. Cuts specified with two numbers (e.g., 50/100) indicate that sieves were used at the high and low end of the size range to bracket it between two approximate values. Cuts specified with "/F" indicate that a sieve was used to constrain the large end of the range, while no constraint was made at the small end (all fines = F were included). Spectral reflectance measurements were made on the samples obtained from both sources. The measurements agreed very well, indicating the uniform quality of the materials from each supplier. As a result, only one (the WM powder) was selected for full evaluation.

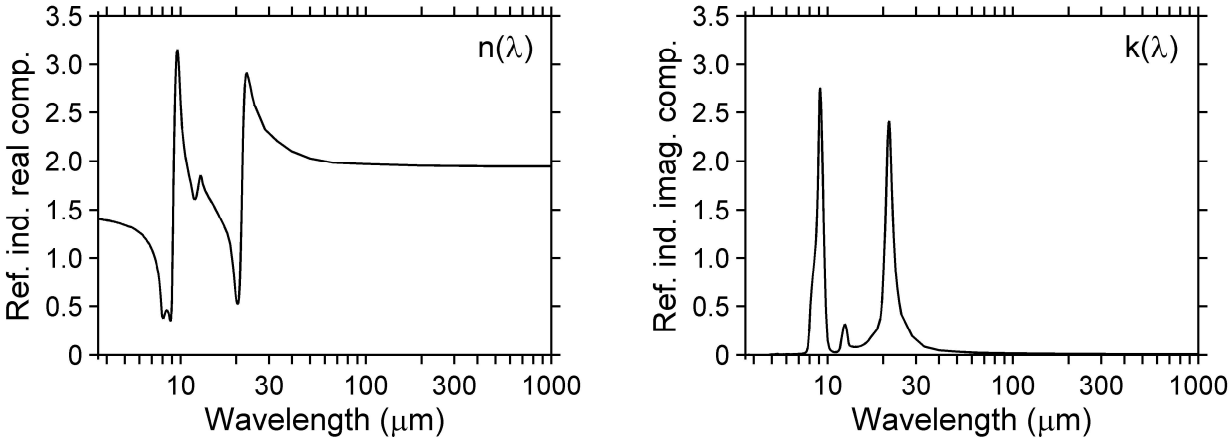


Figure 5 – Plots of n(λ) and k(λ) for fused silica, plotted from the values tabulated by Zolotarev [14]. The sources of the individual data are described in that reference.

Figure 6 contains data describing the morphology of the fused silica samples. The particle size distributions were measured using the scattering instrument. As expected, they show a relatively sharp cutoff at large particle sizes for all samples. Conversely, the /F samples show a gradual decline in fine particle population, while the 50/100 and 100/200 samples show a sharper drop for small particles, which does not extend as far as the /F material.

The central portion of Fig. 6 shows a small set of particle image collected with the automated microscope (at top), and an SEM image of some particles sampled from the 325/F size fraction. The particles appear as elongated shards, and this is confirmed by the circularity histograms plotted at the right side of Fig. 6, which were measured from a much larger ensemble of particles, and which show typical circularities of about 0.8 (circularity is defined as the perimeter of a circle having the same area as the measured particle, divided by the actual perimeter of the particle). The SEM image demonstrates that, in the undisturbed dry state, the fine particles are often adhered to the larger ones. Measurements made using the sizing/shaping instruments use disaggregation mechanisms (air blast, immersion in liquids containing surfactants, ultrasonication) to minimize this effect during size/shape measurements.

Figure 7 shows x-ray tomographic data collected from the WM100/200 powder. The material was contained in a quartz capillary tube having an 800-µm internal diameter. The plotted images were obtained by displaying the selected horizontal and vertical planes within the three-dimensional tomographic dataset. Inspection of the images indicates the packing within the solid, which can eventually be used to generate a direct measurement of the pair distribution function. They also show consistency with the shape profile measured using microscopy.

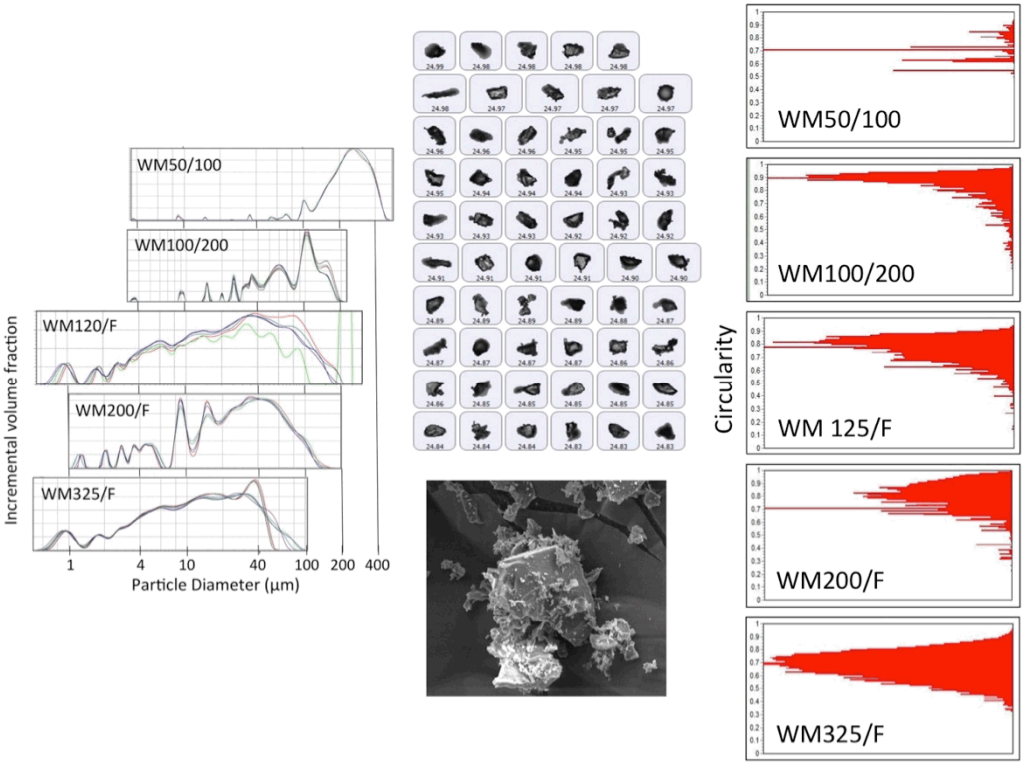


Figure 6 – Morphological data collected from the fused silica particles. They consist of (left) particle-size distributions measured using optical scattering; (center) particle images collected using automated microscopy (above) and SEM (below); and shape distributions measured from the full microscopy dataset.

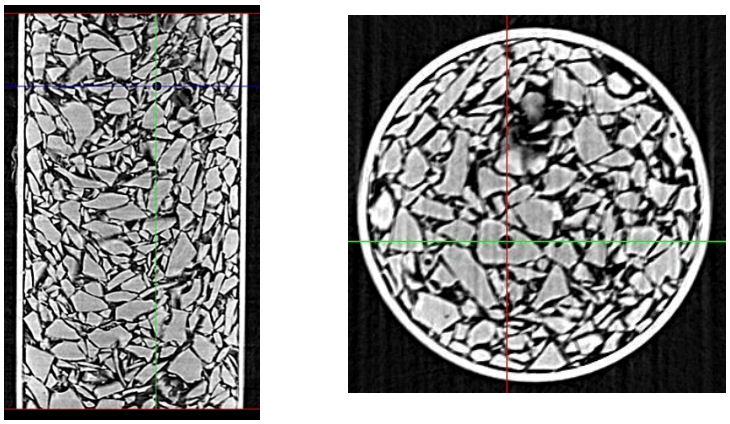

Figure 7 – XRT imagery of the WM100/200 powder displayed as a vertical (left) and horizontal (right) slice through the 3-dimensional dataset.

The reflectance spectra of the fused silica materials are shown in Fig. 8, where they are overlaid with fits made by the RT model. The spectra show bands dominated by surface reflectance (e.g., Restrahlen feature near 9 µm) and those caused by volumetric scattering (e.g., band at 11 µm), which increase with fine particle concentration. General rules

describing the occurrence of these and other behaviors as a function of n and k have been described by Moersch and Christiansen (Reference 2).

Figure 8 shows excellent agreement between the model results and the measured data. In this case, the modeling was performed in the forward direction, where the measured size distributions of Fig. 6 were used as input. The model is based on the assumption that the particles are spheroids and it also used the circularity generated from the shape data as an input. Reference 9 describes the model in detail, and presents further results of its use. Notably, the model was also used in the inverse direction, where it accurately calculated the size distributions from fits of the spectral data.

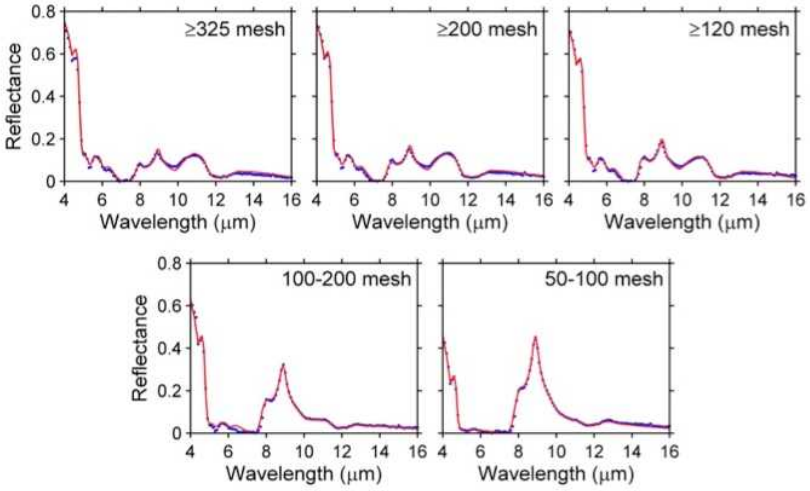


Figure 8 – Plots of the measured diffuse reflectance (red) of the fused silica systems, overlaid with forward model results of their reflectance (blue).

### 3.2 Step 2 – Mildly birefringent system

Crystalline α-$Al_2O_3$ (sapphire) was selected as the material to be used as the mildly birefringent medium. Sapphire is a negative uniaxial crystal with a birefringence ($n_o - n_e$) of 0.008 at 5-μm wavelength. A source of spectral n and k values spanning the full long-wave infrared has not been identified, and, thus, that material is being measured now using spectral ellipsometry.

Particulate single-crystal sapphire was obtained from Sumitomo Chemical (Osaka Japan), where they are manufactured by an aluminum alkoxide hydrolysis process. The particles, classified as their "Advanced Alumina Product" were purchased having nominal diameters of 1.5, 3.0, and 18 μm. Figure 9 contains the relevant morphological data for them. The scattering data demonstrate that the alumina particles are much more uniform in size than the fused silica. The sample images (3 μm particles) from the microscopic data suggest that the particles are nearly spherical in shape, and this is substantiated by the averaged circularity plots, at the right of Fig. 9, which show strong peaks at values of nearly 1. The SEM image of the 18-μm particles shows that the shape is actually polyhedral, with evident facets of the single crystals. Figure 10 contains XRT images of a packed volume of 18- μm particles, underscoring the dense packing of those circular solids.

Figure 11 contains a plot of the directional-hemispherical reflectance of the three particle sizes. They show a particularly strong area of size dependence in the region of a 12.5-μm resonance. The birefringence-enabled version of the model has not been tested against this material, pending completion of the n and k measurements.

## 4. SUMMARY AND CONCLUSION

The results presented here provide a snapshot of progress in a comprehensive effort to generate and characterize model material systems for use in developing and testing RT models of the reflectance of aggregate solids. New measurement techniques are allowing the test media to be characterized at an unprecedented level of detail, which should facilitate model development here and elsewhere. The work is motivated by the needs of HSI, any other technology that relies on reflectance data. This effort is a component of a larger body of work that is funded by the NNSA HARD Solids program, which was described in several talks associated with this session.

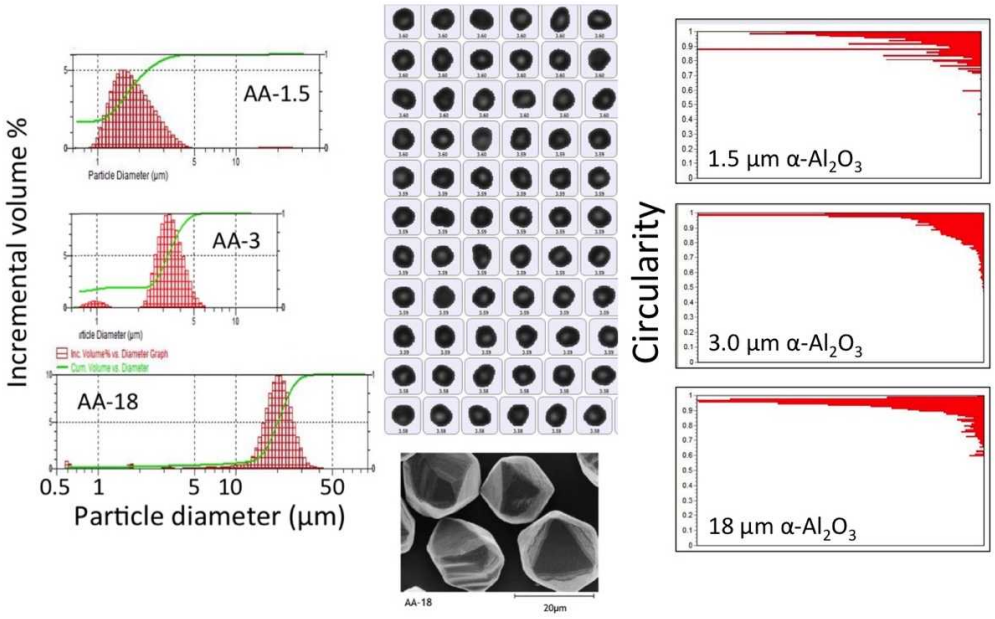


Figure 9 – Morphological data (of the same type as in Fig. 6, measured for the α-alumina powders.

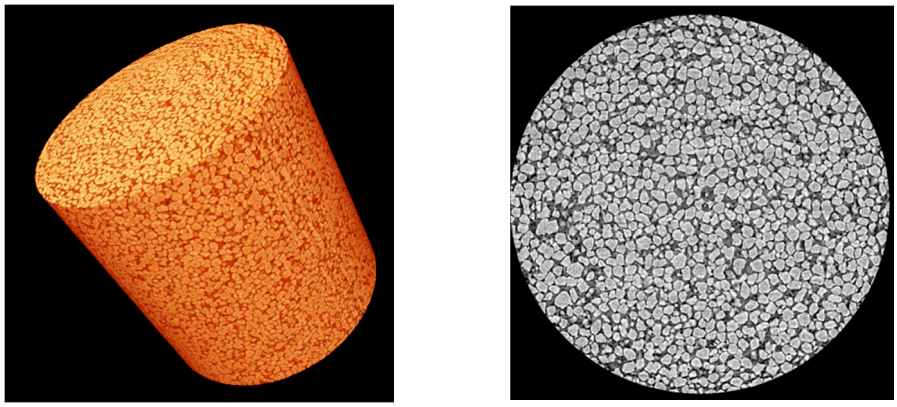

Figure 10 – Representative XRT images of a cylindrical area in the interior of a packed bed of the 18-µm diameter alumina particles.

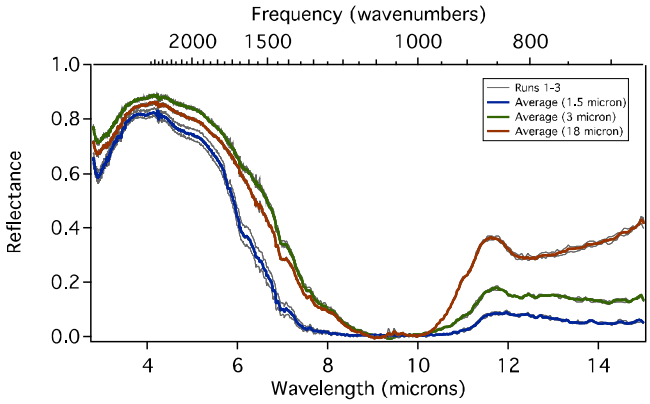


Figure 11 – Directional-hemispheric diffuse reflectance measurements of the alumina powders.

## ACKNOWLEDGEMENTS

The research described in this paper was supported by the U.S. Department of Energy (DOE) National Nuclear Security Administration (NNSA) Office on Nonproliferation and Verification Research and Development (DNN R&D). Sandia is a multi-program laboratory operated by Sandia Corporation, a wholly owned subsidiary of Lockheed Martin Company, for the U.S. Department of Energy's National Nuclear Security Administration under contract DE-AC04-94AL85000.

## REFERENCES

[1] Chang, [Hyperspectral Imaging: Techniques for Spectral Detection and Classification], Springer US, New York & Philadelphia (2003).
[2] Moersch, J. E., and Christensen, P. R., "Thermal emission from particulate surfaces: A comparison of scattering models with measured spectra," J. Geophys. Res. 100(E4), 7465-7477 (1995).
[3] Salisbury, J.W. and Wald, A., "The role of volume scattering in reducing spectral contrast of Restrahlen bands in spectra of powdered minerals, Icarus, 96, 121-128 (1992).
[4] Salisbury, J.W. and Eastes, J.W. "The effect of particle size and porosity on spectral contrast in the mid-infrared", Icarus, 64, 586-588 (1985).
[5] Hunt, G.R. and Logan, L.M., "Variation in single particle mid-infrared emission spectrum with particle size", Appl. Opt., 11, 142-147 (1972).
[6] Hunt, G.R. and Vincent, R.K., "The behavior of spectral features in the infrared emission from particular surfaces of various grain sizes", J. Geophys. Res., 73, 6039-6046 (1968).
[7] Vincent, R.K. and Hunt, G.R., "Infrared reflectance from Mat Surface", Appl. Opt., 7, 53-59 (1968).
[8] Beiswenger, T. N., Myers, T. L., Brauer, C. S., Su, Y.-F., Blake, T. A., Ertel, A. B., Tonkyn, R. G., Szecsody, J. E., Johnson, T. J., Smith, M. O., and Lanker, C. L., "Experimental effects on IR reflectance spectra: particle size and packing," Proc. SPIE 9840-17 (2016).
[9] Reichardt, T.A. and Kulp, T.J., "Radiative transfer modeling of surface chemical deposits", Proc. SPIE 9840-21 (2016).
[10] Mackowski, D.W., "Exact solution for the scattering and absorption properties of sphere clusters on a plane surface", J. Quant. Spectrosc. Radiat. Trans., 770-788, (2008).
[11] Percus, J.K. and Yevick, G.J. "Analysis of classical statistical mechanics by means of collective coordinates", Phys. Rev. 110 (1958).
[12] https://en.wikipedia.org/wiki/Radial_distribution_function
[13] Leonard Hanssen, private communication.
[14] Zolotarev, V. M., "Study of quartz glass by differential Fourier transform IR reflection spectroscopy: Bulk and surface properties," Optics and Spectrosc. 107(5), 754-767 (2009).